An Innovative Single-Cell-Based Injection Method to Improve Efficiency and Reliability of MMC With Low Implementation Burden

Davide D'Amato, *Member, IEEE*, Riccardo Leuzzi, *Member, IEEE*, and Vito Giuseppe Monopoli, *Senior Member, IEEE*

***Abstract*—Modular multilevel converters are increasingly gaining popularity in various high-voltage and high-power applications. However, their operation poses some technical challenges in implementing the control system, including issues, such as balancing submodule capacitor voltages and mitigating circulating currents. The presence of circulating currents leads to additional power losses, increases thermal stress on the power devices, and shortens their lifetime. This article introduces an innovative control technique to eliminate circulating currents by injecting a low-frequency alternating signal into a single submodule of each converter arm. The proposed method not only addresses circulating current mitigation but is also able to reduce capacitor voltage ripple and peak arm current, thereby enhancing the overall converter's lifespan and efficiency. Results of experimental tests on a seven-level converter are presented to prove the effectiveness of the proposed technique and compare its performance with existing state-of-the-art approaches.**

***Index Terms*—Circulating current, efficiency, modular multilevel converter, signal injection, voltage ripple.**

I. Introduction

THE modular multilevel converter (MMC) is recognized as a promising candidate for many high- and medium-voltage applications due to its numerous features, such as improved output waveform quality, modularity, and scalability to different voltage and power levels, fault-tolerant operation, etc. [1], [2]. The MMC can have many variants based on the type of the submodule, such as half-bridge (HB), full-bridge, or version of FBSM called unidirectional-current FBSM (UC-FBSM), which is utilized in many MVDC applications [3]. The MMC operation, however, poses technical challenges due to its structure, which consists of two arms per phase and a single dc port. These challenges include submodule capacitor voltage balancing and circulating current regulation, two phenomena that are closely related [4]. Although the circulating current is part of the converter's internal dynamics and has no influence on the output voltages and currents, it produces increased capacitor voltage ripple in the submodules as well as extra power losses both in the power devices and in the arm inductors [1].

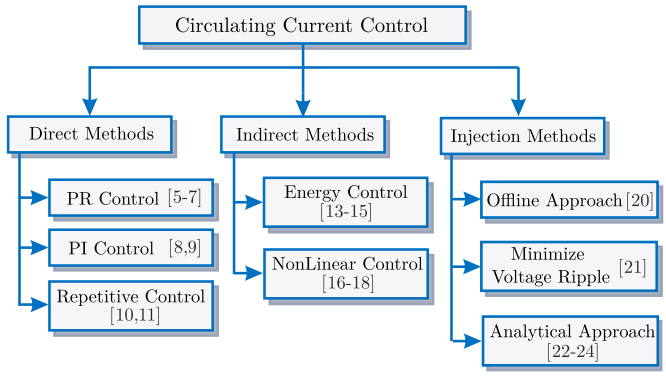

Fig. 1. Classification of circulating current control methods.

In recent years, several studies have been carried out on the mitigation of circulating currents in the MMC, which can be broadly distinguished into direct and indirect techniques according to the selected approach, as shown in Fig. 1. Direct methods are the most widespread and used in many industrial and research fields. These techniques aim at reducing the circulating current through a dedicated feedback loop developed either in the α-β stationary reference frame employing proportional–resonant (PR) regulators [5], [6], [7] or in the synchronous reference frame d-q with proportional–integral (PI) controllers [8], [9]. A repetitive control algorithm has also been proposed in [10] and [11] to suppress the circulating current and its harmonic components. Although these control techniques have been proven to be very effective in reducing the circulating currents, they present the major drawback of only ensuring good tracking and disturbance rejection capabilities at the design frequency [11]. In Li et al.'s [5] work, a dedicated resonant controller is required for each harmonic component of the circulating current being compensated and an additional control loop must be included for capacitor voltage balancing purposes. However, among the

Manuscript received 23 January 2024; revised 11 May 2024; accepted 22 June 2024. Date of publication 5 July 2024; date of current version 4 September 2024. This study was carried out within the NEST - Network 4 Energy Sustainable Transition (D.D. 1243 02/08/2022, PE00000021) and received funding under the National Recovery and Resilience Plan (NRRP), Mission 4 Component 2 Investment 1.3, funded from the European Union - NextGenerationEU. This manuscript reflects only the authors' views and opinions, neither the European Union nor the European Commission can be considered responsible for them. Plexim GmbH supported this work by granting the PLECS academic software sponsorship. Recommended for publication by Associate Editor F. Dijkhuizen. *(Corresponding author: Davide D'Amato.)*

The authors are with the Department of Electrical and Information Engineering, Politecnico di Bari, 70126 Bari, Italy (e-mail: davide.damato@poliba.it; riccardo.leuzzi@poliba.it; vitogiuseppe.monopoli@poliba.it).

Color versions of one or more figures in this article are available at https://doi.org/10.1109/TPEL.2024.3423690.

Digital Object Identifier 10.1109/TPEL.2024.3423690

direct techniques, PR controllers perform well in a stationary α-β framework, allowing effective management of circulating current even when the grid is unbalanced. Unlike PI controllers in the d-q synchronous system, which require a more complex configuration under unbalanced conditions, PR-based structures simplify control because a dual scheme is not required to handle positive and negative sequences [6]. Furthermore, the introduction of coordinate transformations increases control complexity, particularly in the case of unbalanced operations [12]. Such rotating references are difficult to obtain for single-phase systems and require modifications for the unbalanced conditions of three-phase systems.

On the other hand, indirect methods balance the submodule capacitor voltages by acting on the total energy stored of the two converter arms as the primary control channel; as a result, the circulating current is reduced as a secondary effect [13], [14], [15]. Among the indirect control methods, nonlinear techniques such as model predictive control can also be classified, where through accurate dynamic modeling of the converter, different control targets can be pursued at the same time [16], [17], [18]. However, indirect methods tend to be less effective than direct techniques in reducing the circulating current [19], being the model accuracy crucial to these approaches, which are also sensitive to changes in parameters and disturbances in the system. Moreover, the large number of control objectives in the MMC internal dynamics makes it difficult to develop efficient predictive algorithms since cost function tuning and its weighting coefficients may be complex to select.

Circulating current control methods based on an injection signal have been recently proposed and investigated in the literature. This family of control approaches uses a purposely designed circulating current waveform to minimize both the rms of circulating current and the voltage ripple of the submodules of the MMC [20], [21], [22], [23], [24]. Picas et al. [20] presented an offline algorithm to compute two distinct optimized circulating current signals; one consisting solely of the second harmonic component, while the other also included the fourth harmonic component. A signal related to the optimal circulating current is then injected into the reference voltages of the output current controller to suppress specific harmonics in the submodule capacitor voltage ripple. However, an extensive lookup table including the amplitude and phase of the current as a function of the modulation index is required to generate the injection signal calculated with an offline genetic algorithm optimization. The algorithm considers all possible operating conditions of the converter and requires a long time to complete the minimization. A second drawback is that solutions found for high values of the modulation index tend to operate the submodules in the overmodulation region. While the achieved capacitor voltage ripple minimization can be beneficial, overmodulation requires careful consideration of both implementation and stability aspects. In Pou et al.'s [21] work, minimizing the submodule capacitor voltage ripple is the primary target to control the second-harmonic component of the circulating current. However, the circulating current is not suppressed and the increased thermal stress that the injection of the optimized circulating current may cause in the converter is not discussed. A closed-loop control technique based on the injection of second-order circulating current is presented in Wang et al.'s [22] work and uses real-time measures of the phase currents, the phase angle of the output voltages, and the instantaneous values of the modulating signals to calculate circulating current injection signals aimed at pursuing different performance targets. The authors introduce an analytical model to understand the impact of the injection on both submodule capacitor voltage ripple and rms arm current and use it to select the better injection ratio. In this way, the authors avoid using extensive lookup tables, and the circulating current closed-loop control is implemented using a conventional PR controller. However, no analysis was conducted on the sensitivity of the proposed analytical model to parametric variations.

A detailed investigation of the effects of the injection of second-order harmonic components of the circulating current in the modulating signals of an MMC has been carried out in Li et al.'s [23] work. The authors provide guidelines on how circulating current control can affect the performance of the MMC, deriving useful analytical expressions to identify the optimal amplitude and phase angle of the injected signal to pursue different control objectives. A feedforward method is implemented in Wang et al.'s [24] work to reduce the second-order harmonic component of the circulating current by injecting the second harmonic voltage into the reference signals, using instantaneous measurement of both the output and the dc currents. The method employs an analytical model based on the harmonic components of the arm current initially introduced in Ilves et al.'s [25] work. However, the proposed analytical approach has been implemented neither in simulation nor experimentally. Results are obtained with an approximated analytical model assuming only the second harmonic component in the circulating current.

In this work, a single-cell-based injection (SCBI) method is presented that employs only a single submodule per arm as a compensator for the harmonic components of the circulating current, aiming to achieve precise mitigation of the circulating current and reduction of the submodule voltage ripple with a simple but effective feedforward control action. Compared to other methods proposed in the literature, the novel contribution of this injection technique is to leverage the direct measurements of the two arm currents to obtain the instantaneous value of the circulating current and inject all the low-frequency harmonics of the circulating current, being limited only by the bandwidth of the current sensors, avoiding inaccuracies due to the estimation process, frequency fluctuations, and with a minimal impact on the converter operation in terms of power losses. The information and measurements of the arm currents of the MMC are generally available and accessible in the converter for the implementation of capacitor voltage balancing strategies; therefore the proposed circulating current reduction method does not require additional sensors. In addition, the proposed technique is a simple real-time strategy that does not rely on lookup tables or coordinate transformations, achieving improved performance with a lower implementation burden compared to existing techniques. Furthermore, if the submodule in charge of injection should fail, potentially compromising the fault-tolerance capability of the converter, this eventuality is easily resolved in the proposed technique due to its inherently simple implementation via a feedforward action. Indeed, this type of

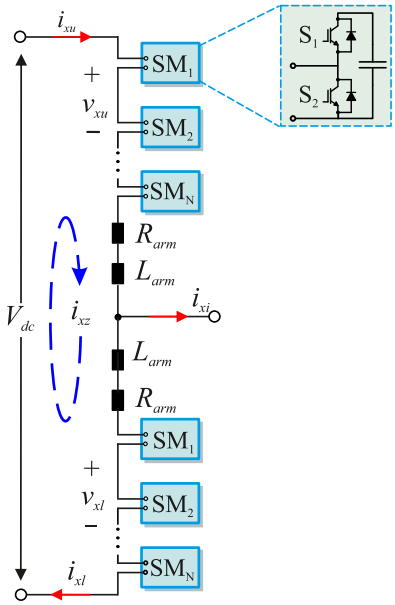

Fig. 2. Generic phase x of the MMC, including the schematic of the submodule.

control can be easily transferred to any remaining submodules without any change in performance.

This article provides a deeper insight into the proposed technique first discussed in D'Amato et al.'s [26] work by presenting both more details on the theoretical aspects and the results of an exhaustive campaign of simulation and experimental tests proving that the SCBI strategy greatly reduces both the circulating current and the ripple of submodule capacitor voltages. In order to provide objective evidence of the effectiveness and performance improvement of the proposed solution, the SCBI approach was evaluated and compared in simulation with three other different controls, one for each family (direct, indirect, and injection methods), to develop a more complete and comprehensive comparison with the technique. In addition, the circulating current PR control [6] was implemented to compare the proposed technique through laboratory experimental tests conducted under the same operating conditions. The rest of this article is organized as follows. Section II presents the main equations describing the circulating current flowing in the MMC arms. Section III introduces the proposed injection method, whereas its effects on the performance of the MMC are described in Section IV. Section V describes the results of simulations performed under different operating conditions for all implemented techniques. Experimental tests are carried out in Section VI to assess the performance of the proposed method in comparison with the conventional PR-based control. Finally, Section VII concludes this article.

II. Circulating Current

The generic phase-leg circuit of an MMC is depicted in Fig. 2, in which each arm consists of N HB submodules in series with the arm inductor L_{arm}. To simplify the analytical treatment, the generic phase x of the converter is considered, but all equations are extendable to the three-phase case. The output and circulating currents can be expressed as a function of the upper and lower arm currents, namely i_{xu} and i_{xl} (with $x = a, b, c$), as shown in the following:

$$i_{xi} = i_{xu} - i_{xl} \tag{1}$$

$$i_{xz} = \frac{i_{xu} + i_{xl}}{2} = i_{xz}^{\text{dc}} + i_{xz}^{\text{ac}}. \tag{2}$$

The circulating current mainly consists of a dc component and an ac component, as shown in (2). The dc part, i_{xz}^{dc}, is responsible for the active power flow through the converter and is equal to one-third of the dc-side current in a three-phase MMC during balanced operation. Indeed, for low rms values of the ac component of the circulating current i_{xz}, the dc component can be expressed as the sum of the arm currents divided by two [25], as shown in the following:

$$i_{xz}^{\text{dc}} = \frac{1}{2} \cdot (i_{xu} + i_{xl}). \tag{3}$$

The ac component, i_{xz}^{ac}, on the other hand, is due to the interaction of the arm voltages and currents and does not contribute to the active power flow [24]. It can be expressed in terms of its harmonic components, each with amplitude $I_{xz,n}$ and phase angle $\theta_{xz,n}$ where n indicates the harmonic order

$$i_{xz}^{\text{ac}} = \sum_{n=1}^{\infty} I_{xz,n} \sin(n\omega t + \theta_{xz,n}). \tag{4}$$

Indeed, the ac part of the circulating current is generated from the phase ripple voltage $\Delta v_{x,n}$ calculated as the sum of each arm voltage ripple [4], thus the nth harmonic component in this circulating current can be also expressed as follows:

$$i_{xz,n}^{\text{ac}} = \frac{\Delta v_{x,n}}{jn\omega 2L_{\text{arm}}}. \tag{5}$$

The denominator of (5) is the arm reactance at the corresponding harmonic frequency.

III. SCBI Method

The proposed injection technique aims at suppressing the ac component of the circulating current calculated in (4). To this purpose, an ac signal directly proportional to the ac component of the circulating current is injected into the reference voltage of a single submodule per arm that acts as a compensator for the total circulating current. All the other submodules in the arm continue to operate normally, generating the voltage levels required for the converter operation. The main idea is to implement a simple and low-computational-cost method for suppressing the circulating current, considering all low-frequency harmonics of the circulating current in the injected signal. The SCBI method not only mitigates the circulating current but also reduces the voltage ripple across all submodule capacitors of the MMC and the rms value of the arm currents. As a result, it leads to improved performance in contrast to the conventional PR circulating control. Moreover, the SCBI approach minimizes losses and improves the overall converter performance without

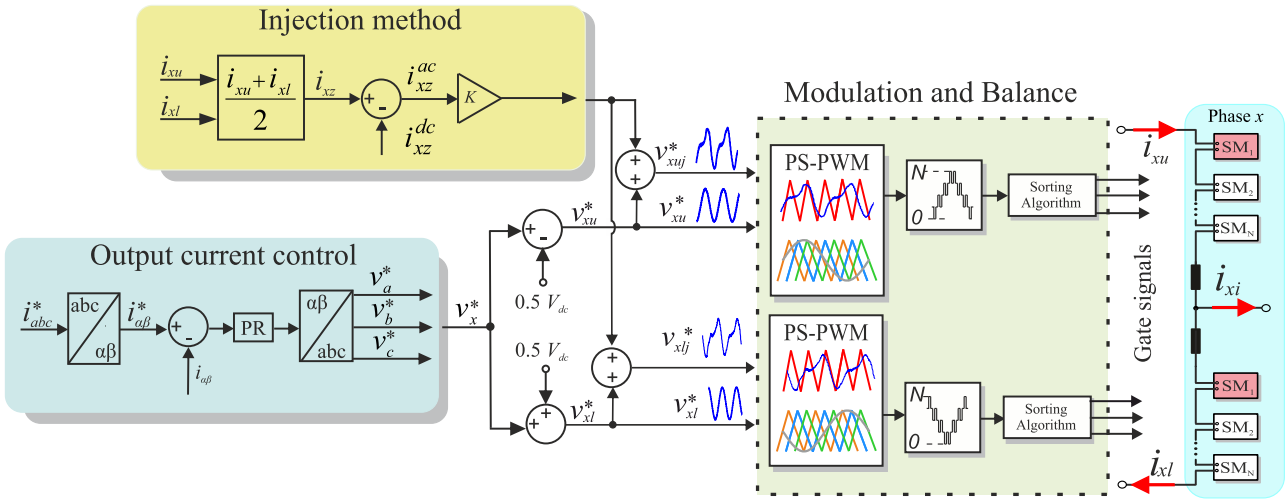

Fig. 3. Simplified block diagram of the proposed circulating current suppression injection scheme.

requiring to oversize the compensating submodule or to derate the converter operation, as shown in the following sections.

A. Control Structure

The block diagram of the proposed SCBI technique is depicted in Fig. 3. The injection signal is implemented in the form of a feedforward control action and is added to the modulating signal of one submodule per arm, which in turn is calculated by the output current control loop. The circulating current signal i_{xz} is derived from the measured instantaneous values of the arm currents using (2). The dc component of the circulating current is related to the active power flow through the converter; therefore, i_{xz}^{dc} can be estimated as one-third of the dc-bus current i_{dc}, which in turn is calculated through the instantaneous power balance between the ac and dc side of the converter, assuming negligible losses [27]

$$i_{\mathrm{dc}} = \frac{\sum p_x}{V_{\mathrm{dc}}} = \frac{\sum v_{xi}^{*} i_{xi}}{V_{\mathrm{dc}}} \tag{6}$$

where p_x is the instantaneous power and v_{xi}^{*} is the reference voltage of phase x. A signal proportional to i_{xz}^{ac} is then added to the modulating signal of the compensating submodule, which then drives the devices to generate a current with an opposite sign than the actual circulating current. A proportional gain K is introduced to regulate the amplitude of the injected signal. The proposed solution avoids the need for a dedicated controller for each frequency component of i_{xz} to be canceled, as in conventional PR approaches, therefore reducing system complexity and improving suppression accuracy. Furthermore, the number of compensated harmonic components is only limited by the bandwidth of the current sensors and the sampling time of the digital control system.

B. Definition of Gain K

The definition of the proportional gain K comes from the analysis of the mathematical model of the circulating current derived by applying the KVL on the MMC phase-leg circuit of Fig. 2

$$2L_{\mathrm{arm}} \frac{di_{xz}}{dt} = V_{\mathrm{dc}} - (v_{xu} + v_{xl}) \tag{7}$$

where v_{xu} and v_{xl} are the upper and lower arm voltages, respectively. By substituting i_{xz} with (2), it is possible to rewrite (7) as

$$2L_{\mathrm{arm}} \left(\frac{di_{xz}^{\mathrm{ac}}}{dt} + \frac{di_{xz}^{\mathrm{dc}}}{dt} \right) = V_{\mathrm{dc}} - (v_{xu} + v_{xl}). \tag{8}$$

Being i_{xz}^{dc} constant at steady state, its derivative is zero, and (8) can simplified as

$$2L_{\mathrm{arm}} \frac{di_{xz}^{\mathrm{ac}}}{dt} = V_{\mathrm{dc}} - (v_{xu} + v_{xl}) = v_{xz} \tag{9}$$

where v_{xz} represents the voltage that is responsible for the ac part of the circulating current and consists of several harmonic components. This voltage is calculated as the product of current harmonics and the arm's reactance at the corresponding frequency. Therefore the injected voltage v_{xz}^{*} can thus be expressed as

$$v_{xz}^{*} = K \cdot i_{xz}^{\mathrm{ac}} = \sum_{n=1}^{\infty} [n\omega L_{\mathrm{arm}} I_{xz,n} \sin(n\omega t + \theta_{xz,n})]. \tag{10}$$

Based on (10), it is possible to define the gain K as related to the overall harmonic impedance of the arm. The proportional gain K is determined through the following analytical model by assuming that the second-order harmonic component of i_{xz}^{ac} is assumed to be dominant and the other harmonics are low enough, the value of K can be calculated as the module of the arm impedance at the frequency 2ω as

$$K = \sqrt{(2\omega \cdot 2L_{\mathrm{arm}})^2 + 4R_{\mathrm{arm}}^2}. \tag{11}$$

In the next section, the value of gain K is verified through simulations by evaluating the effects of the proposed injection technique on the overall performance of the converter.

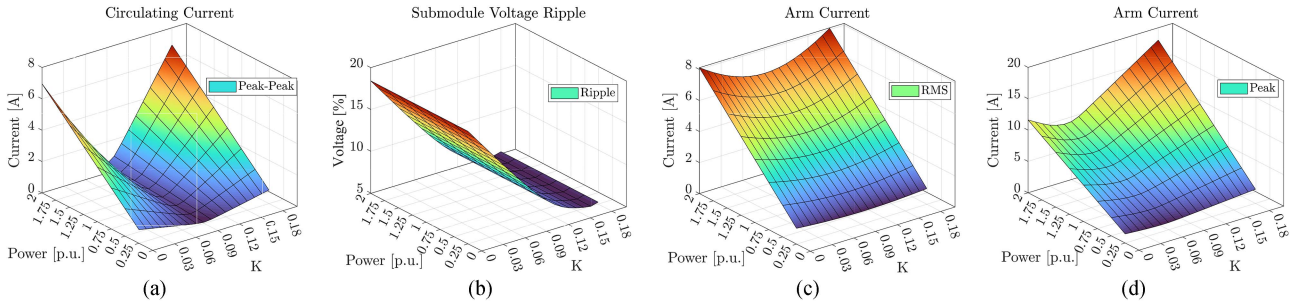

Fig. 4. Effect of the gain K on converter performance at different power levels. (a) Circulating current. (b) Capacitor voltage ripple. (c) Rms. (d) Peak values of the arm current.

TABLE I
MMC PARAMETERS

Parameter	Value
Number of SM N	3
Dc-link voltage V_{DC}	600 V
Output current i_{out}	8 A
Arm inductance L_{arm}	10 mH
SM capacitor C	500 μF
IGBT Rohm (RGCL80TK60DGC11)	(600V–35A @25°C)
Load resistance R	30 Ω
Load inductance L	6.5 mH
Modulation index m	0.8
Fundamental frequency f	50 Hz
Switching frequency f_c	1 kHz

IV. EFFECTS OF SCBI ON MMC PERFORMANCE

The effects of the proposed SCBI method and the proportional gain K on the MMC performance are analyzed through simulation for different power levels ranging from 0.25 to 1.5 per unit. The parameters employed in the model are listed in Table I. The design of the arm inductor of the MMC has been performed by examining the work [25]. Fig. 4(a)–(d) compares the peak-to-peak amplitude of the ac part of the circulating current, the capacitor voltage ripple, the rms value, and the peak value of the upper arm current as a function of K at different power levels with the SCBI technique.The circulating current decreases as K increases up to 0.09, where it reaches a minimum value. Capacitor voltage ripple, rms arm current, and its peak value present a similar trend. The arm currents contain all the harmonic components of the circulating current so that an increase in K will also lead to a reduction in the current rms, thus decreasing the conduction losses of the MMC. However, for greater values of the gain K, an increase in circulating current occurs, which results in an overall increase of rms and peak values of the arm currents.

To analyze the effects that the SCBI method has on the reduction of the circulating current, several simulations are carried out using a simplified injection signal consisting of only the second-order harmonic of the circulating current expressed in (12), in which the phase angle β and the injection signal gain K are varied

$$v_{xz}^{*} = K \cdot I_{xz}(\sin(2\omega t + \beta)). \tag{12}$$

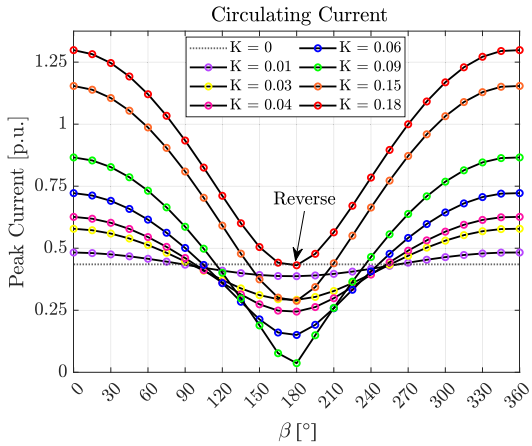

Fig. 5. Amplitude of the second harmonic of the circulating current $I_{xz,2}$ as a function of K and β when the SCBI method is applied. The dotted line refers to the case without control applied.

Fig. 5 shows the amplitude of the second harmonic component of the circulating current as a function of β and K. The variation of the angle β significantly influences the amplitude of the circulating current. In particular, i_{xz}^{ac} decreases as the β phase increases, reaching the minimum when $\beta = 180°$. For higher values of β, the circulating current increases progressively. Furthermore, for $\beta = 180°$, the amplitude of the circulating current decreases as the value of K increases from 0 to 0.09. For $\beta = 180°$ and $K = 0.09$, the minimum amplitude of the circulating current is achieved at 0.03 p.u. However, by further increasing K over 0.09, i_{xz}^{ac} starts to increase again until, for $K = 0.18$, it reaches the same amplitude it had for $K = 0$, when the injected signal is zero, but with opposite phase, i.e., the circulating current has been reversed. This reverse circulating current condition is harmful to the converter because it produces additional losses and distortion on the capacitor strains, eventually leading to instability of the converter control.

V. SIMULATION RESULTS

Several simulations have been conducted to evaluate and compare the performance of the proposed technique under various operating conditions for different power levels, unbalanced conditions, with different load variations, and power factor variations. All displayed results reflect the best tuning that could be achieved for all examined control strategies. The proposed

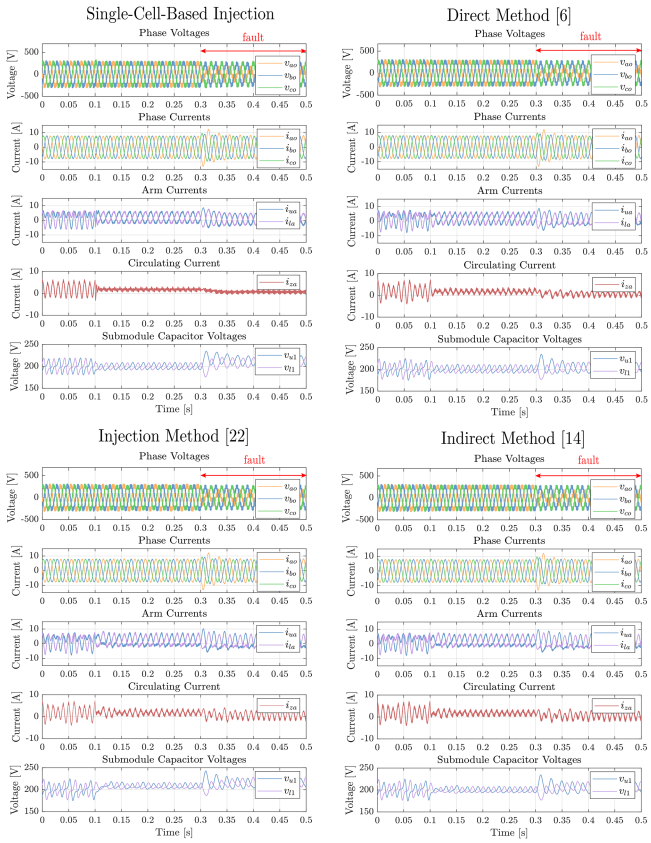

Fig. 6. Simulation results for different control techniques: SCBI, direct method, injection method, and indirect method. A fault occurs on phase A at $t_1 = 0.3$.

technique has been compared with three different control methods from each group, such as direct methods, indirect methods, and injection methods. To compare the performance of the proposed SCBI methods the direct methods based on the PR control described in Li et al.'s [6] work have been implemented, where the circulating current control strategy is designed based on nonideal PR controllers in a α-β steady-state framework. For the indirect technique, the energy control initially proposed in [14] has been selected, which estimates the total energy in the MMC. This approach calculates and controls the total energy stored in each arm of the converter to generate the arm voltage reference, which is then used to drive the semiconductor devices. The injection-based technique, the method proposed in Wang et al.'s [22] work has been used, a closed-loop technique that utilizes second-order circulating current injection. This technique uses real-time measurements of phase currents, the phase angle of output voltages, and instantaneous values of modulation signals to calculate the circulating current injection signals.

To simulate an unbalanced grid condition, a fault on phase A has been applied at $t = 0.3$ s, as shown in Fig. 6. Even under these unbalanced conditions, all techniques demonstrate the ability to reduce circulating current, but with different accuracy. In contrast, the proposed method achieves a significantly greater reduction compared to the other techniques, thanks to its feedforward approach, which does not rely on coordinate transformations. Several simulations at varying power levels

TABLE II
COMPARISON BETWEEN DIFFERENT CONTROL METHODS

Indicator	Injection method [22]	Indirect method [14]	Direct method [6]	SCBI method
Circ. current (peak-to-peak)	55.6%	42.2%	59.6 %	65.6 %
Circ. current (RMS)	65.27%	56.14%	68.25%	72 %
Arm Current (RMS)	5.55%	9.66%	10.94 %	13.47 %
Voltage Ripple	2.35%	3.6%	4.8%	6.12%

have been performed to test all techniques under different operating conditions. Fig. 7 shows the trends in electrical quantities, including output voltages, output currents, circulating currents, and submodule capacitor voltages. All techniques reduce the MMC's circulating current. Subsequently, all techniques have been simulated using an MMC model with a passive load, where resistance load variations of 30, 10, and 40 Ω have been introduced. With changing loads, all techniques experience a certain amount of performance degradation in terms of circulating current reduction. The proposed technique is less affected by the varying load conditions since it keeps reducing the circulating current with good precision, as shown in Fig. 8. All techniques were tested for different power factor values from 0.99 to 0.8, as shown in Fig. 9. The proposed technique reduces the rms value of the circulating current for different power factors managing to provide a reduction of about 70%. In addition, the voltages of the submodule remain balanced with each other according to their reference value.

In addition, it is necessary to specify that the voltage balancing technique based on the sorting algorithm has been implemented in the simulations. This technique works by selecting which submodules to insert or bypass based on the insertion index, the sign of the arm current, and the instantaneous voltage values, ensuring balance regardless of which submodule in the arm compensates for the circulating current. Consequently, it might happen that during the fundamental period of the carrier ($T_c = \frac{1}{f_c}$, where f_c is the switching frequency), the submodule designated to inject the circulating current is not inserted. This effect, due to the implementation of the sorting algorithm, undermines the performance of any implemented technique by reducing the number of submodules with which control action is transmitted.

Results from the simulations presented previously are summarized in Table II. The peak-to-peak value of the circulating current, its rms value, the rms value of the arm currents, and the voltage ripple across the capacitors were considered. All values are expressed as a percentage reduction compared to the case where no control is applied for circulating current reduction where the higher value means a greater reduction.

Fig. 10 compares conduction and switching losses in the MMC submodules for the four control techniques. The switching and conduction losses were calculated as percentages considering the case where no circulating current reduction control is applied. The bar graph provides a detailed breakdown of the losses for each submodule of the upper arm of phase a, obtained by simulation using PLECS and the thermal model of the devices employed in the experimental rig. In the case of

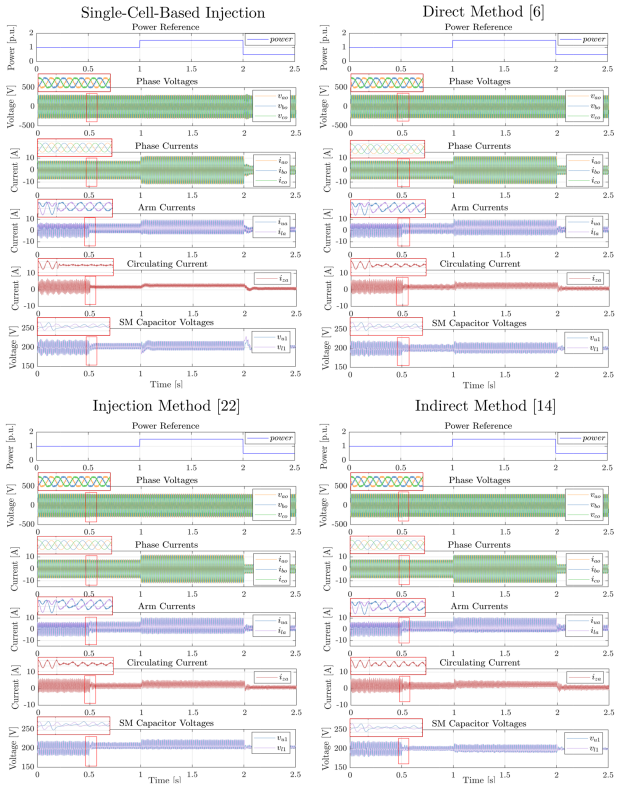

Fig. 7. Simulation results for different control techniques: SCBI, direct method, injection method, and indirect method for different power levels.

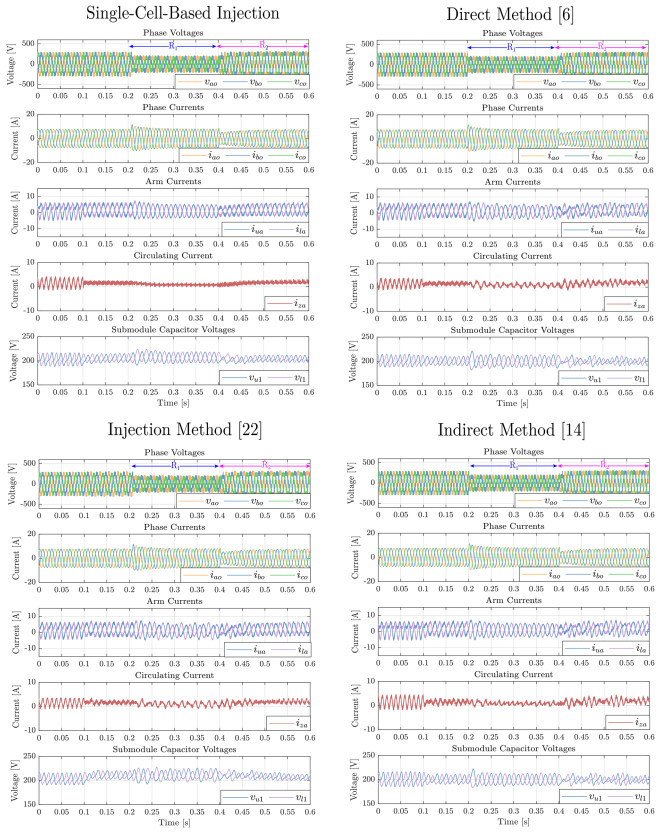

Fig. 8. Simulation results for different control techniques: SCBI, direct method, injection method, and indirect method. At $t_1 = 0.2$ s the resistance load changes from 30 to 10 Ω and in time $t_2 = 0.4$ the load changes from 10 to 40 Ω.

SCBI, injection is performed on SM_1 highlighted in red in the Fig. 10. All of the implemented techniques reduce power losses, and there is no noticeable difference. However, the proposed technique achieves a notable reduction of the submodule losses, approximately 60% lower than in the uncontrolled case. It is worth noticing that, despite the injection being performed only on a single submodule, no significant difference is found in terms of increased losses between the submodule where the injection is applied and those without injection, indicating that oversizing of the submodule is not necessary when the proposed SCBI method is used. Indeed, conduction losses only depend on the rms value of the arm current, which is the same for all the submodules. Furthermore, switching losses are evenly distributed among the submodules when the control strategy is employed.

VI. Experimental Results and Discussion

The experimental tests are performed on the single-phase MMC laboratory prototype shown in Fig. 11(a), whose characteristics are the same as those used for the simulation model listed in Table I. The experimental tests are performed on a passive RL load, connecting it at the center point of the experimental circuit, as shown in Fig. 11(b). The modulation strategy employed is the phase-shifted carrier pulse width modulation, with a switching frequency set to 1 kHz, and the output current is set at 8 A through implementing an output current control. The submodule capacitor voltages are measured for each arm and balanced using the technique described in Dekka et al.'s [28] work, which identifies the submodules to be inserted or bypassed using logic comparators instead of the conventional sorting algorithm [8]. During the experimental tests, effective circulating current mitigation, voltage ripple reduction, and efficiency are measured, and also the dynamic response is evaluated to assess the performance of the proposed SCBI technique. The same tests are carried out by implementing a conventional circulating current control based on a PR regulator to serve as a benchmark for the performance comparison between the two techniques.

TABLE III
Parameters of PR Control and SCBI

Symbol	Description	Value
k_r	Resonant controller gain	250
k_p	Proportional controller gain	8
ω_c	Resonant controller width	0.01
ω_0	Resonant controller frequency	628
K	SCBI gain	0.09

The parameters of the controllers used in the experimental tests of both control strategies are displayed in Table III. The tuning and discretization of the PR controller were investigated in the works [6], [7].

Fig. 12 compares the waveforms of the simulations with those of the experimental results before and after the SCBI is applied, thus validating the simulative model and the choice of gain K with which the proposed technique is implemented.

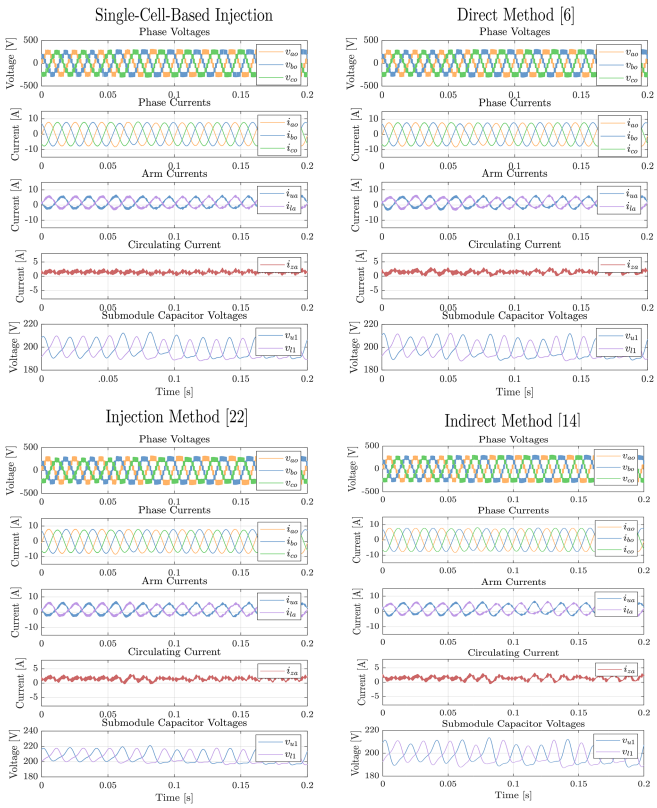

Fig. 9. Simulation results for different control techniques: SCBI, PR control, injection-based, and energy control at different power factor variations at time $t = 0.05$ change from 0.99 to 0.80.

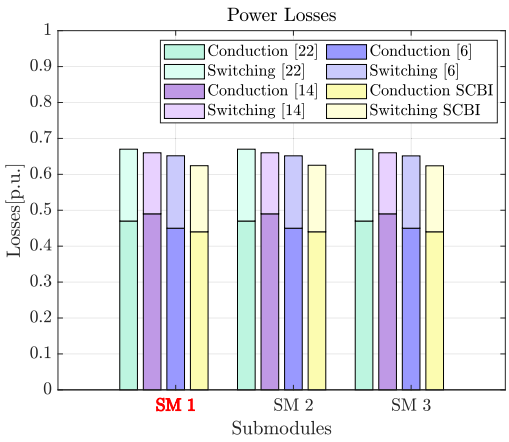

Fig. 10. Histogram of conduction and switching losses for each submodule of the upper arm for the various implemented control techniques.

The waveforms obtained during the experimental tests for a dc-bus voltage of 600 V for the conventional PR control and the proposed injection-based technique are shown in Fig. 13. The circulating current shown in the figure is measured with the oscilloscope as the sum of the currents of the two arms divided by two. The circulating current reaches a peak-to-peak value of 4.3 A when PR control is used, whereas it becomes 3.5 A with the proposed SCBI technique. The rms value of the circulating current drops from 0.8 A with the PR regulator to 0.6 A for the SCBI method. The rms value of the arm current is 3.5 A for PR

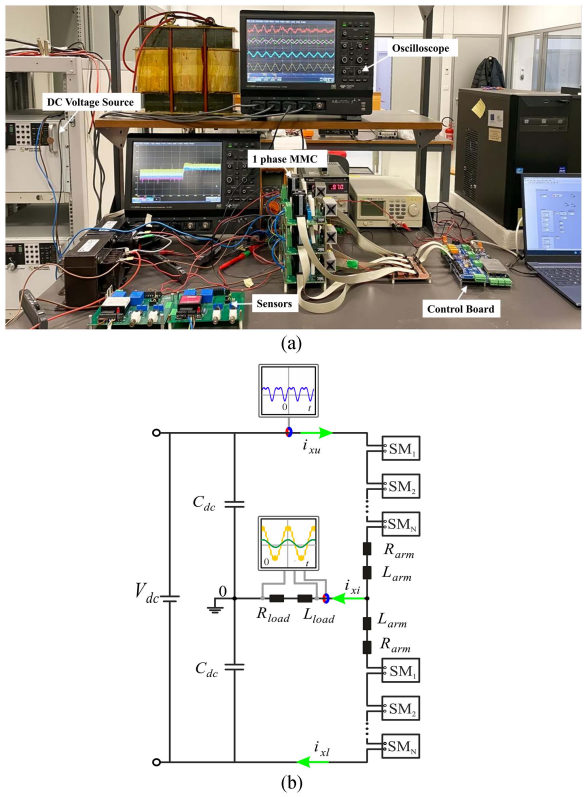

Fig. 11. Seven-level experimental prototype converter. (a) Photograph of the laboratory prototype. (b) Circuit diagram of the laboratory prototype.

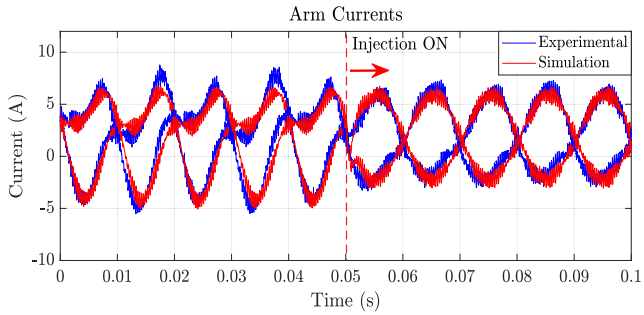

Fig. 12. Comparison of experimental and simulated waveforms of arm currents before and after application of the SCBI technique.

control whereas it reaches a value of 3.3 A by using the SCBI. Fig. 14(a) and (b) depicts the transient waveforms when turning the circulating control on with both techniques, respectively, the PR and the SCBI. Comparing the two graphs, it can be observed that the peak-to-peak value of the circulating current, through the PR control action, is reduced by 45% compared to the case without applying any control.

In contrast, by implementing the SCBI technique, the value is reduced by 55%. The rms value of the circulating current is reduced by 58% when PR control is activated and by 68% with the SCBI enabled.

Fig. 15 illustrates the voltage ripple of the submodule capacitors before and after the reduction of the circulating current for both methods, calculated as the ratio of the peak-to-peak

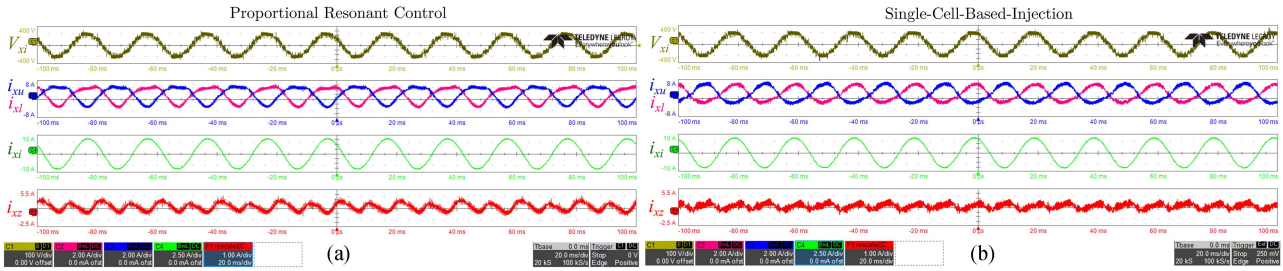

Fig. 13. Experimental waveform of the output voltage V_{xi}, output current i_{xi}, the arm currents $i_{xu,l}$, and the circulating current i_{xz} with (a) PR current control and (b) with SCBI Method.

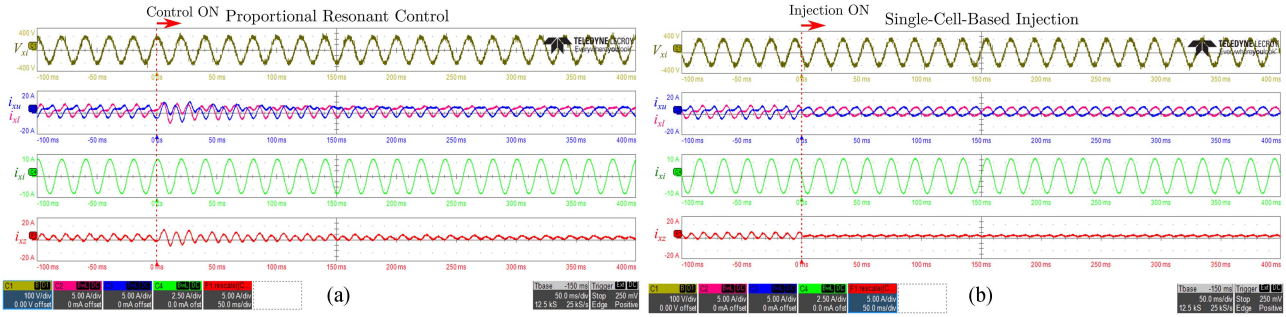

Fig. 14. Experimental waveform of the output voltage V_{xi}, output current i_{xi}, the arm currents $i_{xu,l}$ and the circulating current i_{xz} before and after applying (a) PR circulating control and (b) SCBI method.

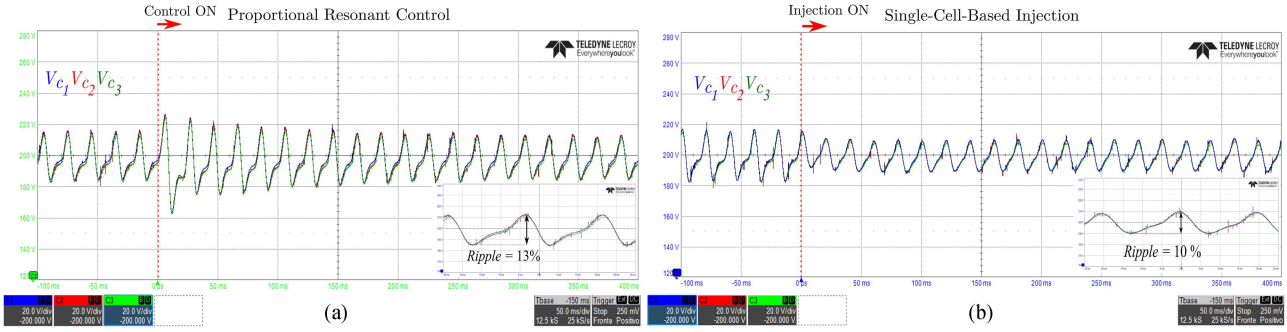

Fig. 15. Experimental waveform of the capacitor voltages of the upper arm before and after applying (a) PR circulating control and (b) SCBI method.

value of the oscillation to the average value. Due to the relatively low capacitance value of the submodules used in the experimental rig (i.e., 500 μF), the initial voltage ripple is quite large (16 %). However, applying both methods results in a noticeable reduction of the voltage ripple by about 3%. The two techniques achieve approximately 13% with PR control and 10% with the SCBI. The submodule capacitor voltage waveforms exhibit spikes; this phenomenon is related to the implementation of the submodule voltage balancing control based on the sorting algorithm. Although the sorting algorithm offers excellent performance, it also increases the device's average switching frequency, resulting in a corresponding increase in unnecessary switching events [29], contributing to increased switching losses and stress on the transistors [30]. In addition, the submodule that performs the compensation does not exhibit a different voltage ripple compared to the others because the effect of the injection and the resulting reduction in circulating current has a global impact on the entire MMC phase, reducing the ripple in all capacitors.

Fig. 16 shows the harmonic spectrum of the measured upper arm current without circulating current control, with PR control, and with the proposed injection technique. The amplitudes of the spectrum harmonics are presented in p.u., with the peak output current of 8 A as a reference. The SCBI technique achieves a better reduction of the second harmonic component than the PR control by decreasing the second harmonic about 41%, thus increasing the efficiency of the converter. The efficiency is measured with a power analyzer for the two techniques for different power levels and is presented in Fig. 17, with P_{in} and P_{out} being the input and output powers, respectively.

The proposed technique has globally higher efficiency than the conventional technique. In particular, at 1 kW, the efficiency achieved with the conventional PR control is 94 147%, while reaching 94 315% with the proposed technique.

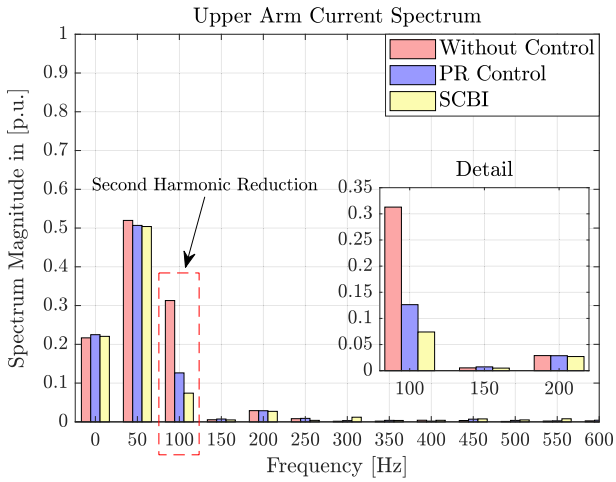

Fig. 16. Harmonic spectrum of the measured upper arm current in three different cases: without any control, with PR control, and SCBI method.

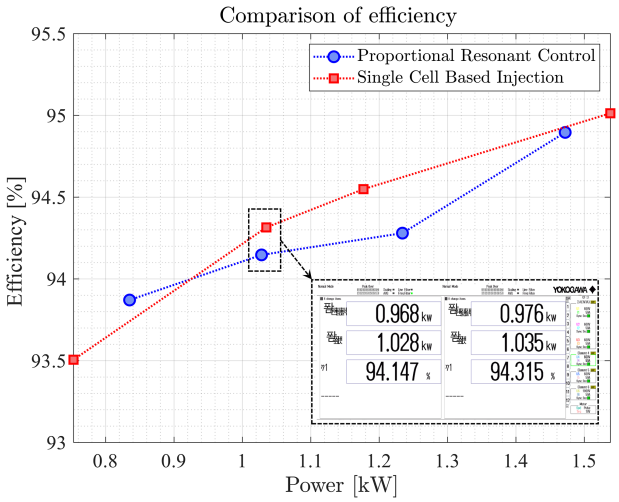

Fig. 17. Measured efficiencies at different power levels of the two techniques in comparison.

TABLE IV
COMPARISON BETWEEN PR CONTROL AND SCBI

Indicator	Without control	PR control	SCBI method
Circ. current (peak-to-peak)	7.8A	4.3A (45%)	3.5A (55%)
Circ. current (RMS)	1.9A	0.8A (58%)	0.6A (68%)
Arm Current (RMS)	3.9A	3.5A (10.3%)	3.3A (15.4%)
Voltage Ripple	16%	13% (3%)	10% (6%)

Results from the experimental test that are presented previously are summarized in Table, for both techniques the percent reduction compared to the case without control is also present (see Table IV).

VII. SUMMARY AND CONCLUSION

In this work, a novel control method for suppressing the ac components of the circulating current in MMCs is proposed, which is based on the injection of a signal proportional to the circulating current itself into a single submodule of each converter arm. To properly tune the proportional gain K of the feedforward action that performs the injection, its effect on the converter operation is simulated and analyzed in various conditions, identifying the optimal value for the minimization of the circulating current. The proposed technique was compared with three control methods, representing each of the main control families, in various operating conditions. The simulation results showed that the new technique effectively reduces the circulating current in all tested scenarios. Furthermore, by reducing circulating current and voltage ripple, the technique allows the converter to be designed with smaller arm inductor values and submodule capacitance. The experimental tests performed on a single-phase, seven-level laboratory prototype to assess its effectiveness and performance show that the proposed technique effectively dampens the circulating current, reduces the submodule capacitor voltage ripple, and improves the converter performance. Experimental results also show that the proposed approach is able to mitigate the losses of the converter by reducing the rms and peak values of the arm currents without requiring to oversize the compensating submodule or downgrade the converter operation. Finally, the proposed solution succeeds in achieving a performance enhancing with a reduced implementation burden in comparison to already existing techniques. In a future step, the implementation and behavior of the proposed control method during internal fault conditions of the MMC can be further investigated. Among these, a different voltage balancing strategy could be utilized to enhance the performance of the proposed technique, reducing the switching frequency of the devices and decreasing the overall converter losses.

REFERENCES

[1] S. Debnath, J. Qin, B. Bahrani, M. Saeedifard, and P. Barbosa, "Operation, control, and applications of the modular multilevel converter: A review," *IEEE Trans. Power Electron.*, vol. 30, no. 1, pp. 37–53, Jan. 2015.

[2] M. Li, X. Jiang, C. Chen, K. Zhang, and J. Xiong, "Fault-tolerant strategy for modular multilevel converters with combined zero-sequence voltage injection," *IEEE Trans. Power Electron.*, vol. 39, no. 7, pp. 8101–8113, Jul. 2024, doi: 10.1109/TPEL.2024.3390421.

[3] Z. Li, Q. Song, B. Zhao, Z. Yu, R. Zeng, and B. Cui, "Analysis of ride-through capability of unidirectional-current MMC with arm current unidirectionality disrupted," *IEEE Trans. Power Electron.*, vol. 39, no. 8, pp. 9257–9267, Aug. 2024.

[4] Q. Song, W. Liu, X. Li, H. Rao, S. Xu, and L. Li, "A steady-state analysis method for a modular multilevel converter," *IEEE Trans. Power Electron.*, vol. 28, no. 8, pp. 3702–3713, Aug. 2013.

[5] Z. Li, P. Wang, Z. Chu, H. Zhu, Y. Luo, and Y. Li, "An inner current suppressing method for modular multilevel converters," *IEEE Trans. Power Electron.*, vol. 28, no. 11, pp. 4873–4879, Nov. 2013.

[6] S. Li, X. Wang, Z. Yao, T. Li, and Z. Peng, "Circulating current suppressing strategy for MMC-HVDC based on nonideal proportional resonant controllers under unbalanced grid conditions," *IEEE Trans. Power Electron.*, vol. 30, no. 1, pp. 387–397, Jan. 2015.

[7] P. Hu, Z. He, S. Li, and J. M. Guerrero, "Non-ideal proportional resonant control for modular multilevel converters under sub-module fault conditions," *IEEE Trans. Energy Convers.*, vol. 34, no. 4, pp. 1741–1750, Dec. 2019.

[8] Q. R. Tu, Z. Xu, and L. Xu, "Reduced switching-frequency modulation and circulating current suppression for modular multilevel converters," *IEEE Trans. Power Del.*, vol. 26, no. 3, pp. 2009–2017, Jul. 2011.

[9] Y. Xu, Z. Xu, Z. Zhang, and H. Xiao, "A novel circulating current controller for MMC capacitor voltage fluctuation suppression," *IEEE Access*, vol. 7, pp. 120141–120151, 2019.

[10] L. Q. He, K. Zhang, J. Xiong, and S. F. Fan, "A repetitive control scheme for harmonic suppression of circulating current in modular multilevel converters," *IEEE Trans. Power Electron.*, vol. 30, no. 1, pp. 471–481, Jan. 2015.
[11] S. Yang, P. Wang, Y. Tang, M. Zagrodnik, X. Hu, and K. J. Tseng, "Circulating current suppression in modular multilevel converters with even-harmonic repetitive control," *IEEE Trans. Ind. Appl.*, vol. 54, no. 1, pp. 298–309, Jan./Feb. 2018.
[12] L. Yang, Y. Li, Z. Li, P. Wang, S. Xu, and R. Gou, "Loss optimization of MMC by second-order harmonic circulating current injection," *IEEE Trans. Power Electron.*, vol. 33, no. 7, pp. 5739–5753, Jul. 2018.
[13] L. Angquist, A. Antonopoulos, D. Siemaszko, K. Ilves, M. Vasiladiotis, and H. P. Nee, "Open-loop control of modular multilevel converters using estimation of stored energy," *IEEE Trans. Ind. Appl.*, vol. 47, no. 6, pp. 2516–2524, Nov./Dec. 2011.
[14] A. Antonopoulos, L. Angquist, and H.-P. Nee, "On dynamics and voltage control of the modular multilevel converter," in *Proc. 13th Eur. Conf. Power Electron. Appl.*, Barcelona, Spain, 2009, pp. 1–10.
[15] Q. Gui, H. Fehr, and A. Gensior, "Energy control of modular multilevel converters for drive applications at low frequency using general averaging," *IEEE Trans. Power Electron.*, vol. 39, no. 5, pp. 5239–5256, May 2024.
[16] J. Yin, N. Dai, J. I. Leon, M. A. Perez, S. Vazquez, and L. G. Franquelo, "Common-mode-Voltage regulation of modular multilevel converters through model predictive control," *IEEE Trans. Power Electron.*, vol. 39, no. 6, pp. 7167–7180, Jun. 2024.
[17] H. Yang and M. Saeedifard, "A capacitor voltage balancing strategy with minimized AC circulating current for the DC–DC modular multilevel converter," *IEEE Trans. Ind. Electron.*, vol. 64, no. 2, pp. 956–965, Feb. 2017.
[18] J. Qin and M. Saeedifard, "Predictive control of a modular multilevel converter for a back-to-back HVDC system," *IEEE Trans. Power Del.*, vol. 27, no. 3, pp. 1538–1547, Jul. 2012.
[19] J. Wei, A. B. Acharya, L. Norum, and P. Bauer, "Comparison of current control strategies in modular multilevel converter," in *Proc. Int. Power Electron. Conf.*, Niigata, Japan, 2018, pp. 2630–2637.
[20] R. Picas, J. Pou, S. Ceballos, J. Zaragoza, G. Konstantinou, and V. G. Agelidis, "Optimal injection of harmonics in circulating currents of modular multilevel converters for capacitor voltage ripple minimization," in *Proc. IEEE ECCE Asia Downunder*, Melbourne, VIC, Australia, 2013, pp. 318–324.
[21] J. Pou, S. Ceballos, G. Konstantinou, V. G. Agelidis, R. Picas, and J. Zaragoza, "Circulating current injection methods based on instantaneous information for the modular multilevel converter," *IEEE Trans. Ind. Electron.*, vol. 62, no. 2, pp. 777–788, Feb. 2015.
[22] J. Wang, X. Han, H. Ma, and Z. Bai, "Analysis and injection control of circulating current for modular multilevel converters," *IEEE Trans. Ind. Electron.*, vol. 66, no. 3, pp. 2280–2290, Mar. 2019.
[23] X. Li, Q. Song, W. Liu, S. Xu, Z. Zhu, and X. Li, "Performance analysis and optimization of circulating current control for modular multilevel converter," *IEEE Trans. Ind. Electron.*, vol. 63, no. 2, pp. 716–727, Feb. 2016.
[24] C. Wang, Q. Hao, and B. Ooi, "Reduction of low-frequency harmonics in modular multilevel converters (MMCs) by harmonic function analysis," *IET Gener. Transmiss. Distrib.*, vol. 8, no. 2, pp. 328–338, 2014.
[25] K. Ilves, A. Antonopoulos, S. Norrga, and H. P. Nee, "Steady-state analysis of interaction between harmonic components of arm and line quantities of modular multilevel converters," *IEEE Trans. Power Electron.*, vol. 27, no. 1, pp. 57–68, Jan. 2012.
[26] D. D'Amato, R. Leuzzi, and V. G. Monopoli, "A single-cell-based injection method for circulating current control in MMC," in *Proc. IEEE Energy Convers. Congr. Expo.*, Nashville, TN, USA, 2023, pp. 2837–2842.
[27] D. Wu and L. Peng, "Analysis and suppressing method for the output voltage harmonics of modular multilevel converter," *IEEE Trans. Power Electron.*, vol. 31, no. 7, pp. 4755–4765, Jul. 2016.
[28] A. Dekka, B. Wu, R. L. Fuentes, M. Perez, and N. R. Zargari, "Evolution of topologies, modeling, control schemes, and applications of modular multilevel converters," *IEEE Trans. Emerg. Sel. Topics Power Electron.*, vol. 5, no. 4, pp. 1631–1656, Dec. 2017.
[29] Y. Li, E. A. Jones, and F. Wang, "The impact of voltage-balancing control on switching frequency of the modular multilevel converter," *IEEE Trans. Power Electron.*, vol. 31, no. 4, pp. 2829–2839, Apr. 2016, doi: 10.1109/TPEL.2015.2448713.
[30] F. Hahn, M. Andresen, G. Buticchi, and M. Liserre, "Thermal analysis and balancing for modular multilevel converters in HVDC applications," *IEEE Trans. Power Electron.*, vol. 33, no. 3, pp. 1985–1996, Mar. 2018, doi: 10.1109/TPEL.2017.2691012.

Davide D'Amato (Member, IEEE) received the M.Sc. and Ph.D. degrees in electrical engineering from Politecnico di Bari, Bari, Italy, in 2019 and 2024, respectively.

He is currently a Research Associate with the Fraunhofer Institute for Silicon Technology, Itzehoe, Germany. His research interests include grid-connected converters, advanced control, and modulation techniques of multilevel converters, and SiC devices.

Riccardo Leuzzi (Member, IEEE) received the M.Sc. and Ph.D. degrees in electrical and information engineering from the Politecnico di Bari, Bari, Italy, in 2016 and 2020, respectively.

He is currently a Research Fellow with the Department of Electrical and Information Engineering at the Politecnico di Bari. His research interests include the control and modulation of multilevel converters for grid and transportation applications, the reliability of power electronics and drives, and the design and control of power electronics converters.

Dr. Leuzzi was a co-recipient of the 2019 Second Prize Paper Award of the Industrial Power Converter Committee of the IEEE Industry Applications Society.

Vito Giuseppe Monopoli (Senior Member, IEEE) received the M.Sc. and Ph.D. degrees in electrical engineering from the Politecnico di Bari, Bari, Italy, in 2000 and 2004, respectively.

He is currently a Full Professor with the Department of Electrical and Information Engineneering, Politecnico di Bari. His research interests include innovative control and modulation techniques for multilevel converters and in general on the analysis of harmonic distortion produced by power converters and electrical drives.

Dr. Monopoli was a co-recipient of the 2021 Best Paper Award of IEEE Industrial Electronics Magazine and the 2023 Best Paper Award of IEEE Industrial Electronics Magazine.